A germline heterozygous dominant negative *IKZF2* variant causing syndromic primary immune regulatory disorder and ICHAD

Henry Y. Lu[1,2], Maryam Vaseghi-Shanjani[1,2], Avery J. Lam[3,4], Mehul Sharma[1,2], Arezoo Mohajeri[5], Jana Gillies[3,4], Gui Xiang Yang[5], Susan Lin[1], Maggie P. Fu[5,6,7], Areesha Salman[5], Ronak Rahmanian[8], Linlea Armstrong[5], Jessica Halparin[1,9], Connie L. Yang[1,9], Mark Chilvers[1,10], Erika Henkelman[11], Wingfield Rehmus[1,12], Douglas Morrison[1,13], Audi Setiadi[1,13], Sara Mostafavi[5,14], Michael S. Kobor[5,7], Frederick K. Kozak[8], Catherine M. Biggs[1,15], Clara van Karnebeek[1,7], Kyla J. Hildebrand[1,15], Anna Lehman on behalf of the Care4Rare Canada Consortium[5], Megan K. Levings[3,4,16], Stuart E. Turvey[1,2,14]

[1]Department of Pediatrics, BC Children's Hospital, The University of British Columbia, Vancouver, BC, Canada
[2]Experimental Medicine Program, Faculty of Medicine, The University of British Columbia, Vancouver, BC, Canada
[3]BC Children's Hospital Research Institute, Vancouver, BC, Canada
[4]Department of Surgery, The University of British Columbia, Vancouver, BC, Canada
[5]Department of Medical Genetics, The University of British Columbia, Vancouver, BC, Canada
[6]Genome Science and Technology Program, Faculty of Science, The University of British Columbia, Vancouver, BC, Canada
[7]Centre for Molecular Medicine and Therapeutics, Vancouver, BC, Canada
[8]Division of Otolaryngology – Head & Neck Surgery, BC Children's Hospital, The University of British Columbia, Vancouver, BC, Canada
[9]Division of Hematology, Oncology & Bone Marrow Transplant, BC Children's Hospital, The University of British Columbia, Vancouver, BC, Canada
[10]Division of Respiratory Medicine, BC Children's Hospital, The University of British Columbia, Vancouver, BC, Canada
[11]Division of Plastic Surgery, BC Children's Hospital, The University of British Columbia, Vancouver, BC, Canada
[12]Division of Dermatology, BC Children's Hospital, The University of British Columbia, Vancouver, BC, Canada
[13]Department of Pathology and Laboratory Medicine, BC Children's Hospital, The University of British Columbia, Vancouver, BC, Canada
[14]Department of Statistics, The University of British Columbia, Vancouver, BC, Canada
[15]Division of Allergy and Clinical Immunology, BC Children's Hospital, The University of British Columbia, Vancouver, BC, Canada
[16]School of Biomedical Engineering, The University of British Columbia, Vancouver, BC, Canada

Correspondence to: Stuart E. Turvey, MBBS, DPhil, FRCPC
BC Children's Hospital
950 West 28th Avenue
Vancouver, BC, V5Z 4H4, Canada
Phone: 604 875 2345 ext. 5094
Email: sturvey@bcchr.ca

Word count: 4107

Reference count: 52

Abstract:

Monogenic defects that impair the control of inflammation and tolerance lead to profound immune dysregulation, including autoimmunity and atopy. Studying these disorders reveals important molecular and cellular factors that regulate human immune homeostasis and identifies potential precision medicine targets. Here, we provide a detailed immunological assessment of a pediatric patient with a recently discovered syndrome causing Immunodysregulation, Craniofacial anomalies, Hearing impairment, Athelia, and Developmental delay (or ICHAD syndrome). The immunodysregulation resulted in autoimmune hemolytic anemia (AIHA) and atopic dermatitis. The patient carried a *de novo* germline heterozygous c.406+540_574+13477dup;p.Gly136_Ser191dup variant in *IKAROS family zinc finger 2* (*IKZF2*), which encodes Helios. This variant led to reduced Helios protein expression and dominant interference of wild-type Helios-mediated repression of the *IL2* promoter. Multi-parameter flow cytometric analyses of patient peripheral blood mononuclear cells revealed strongly impaired natural killer cell differentiation and function, and increased $CD8^+$ T cell activation and cytokine secretion. Strikingly, patient $CD4^+$ T cells were hyperactive, produced elevated levels of nearly all T helper (T_H) cytokines, and readily proliferated in response to stimulation. Patient regulatory T cells (Tregs) developed normally but aberrantly produced high levels of many T_H cytokines. Single-cell RNA sequencing revealed largely normal Tregs (albeit mostly memory), but naïve $CD4^+$ T cells that were more enriched in genes related to activation, proliferation, metabolism, and T_H differentiation. This work describes the immunological phenotype of one of the first reported cases of germline dominant negative Helios deficiency, expands our understanding of the pathogenesis of AIHA on a single cell level, and provides valuable insights into Helios function in a variety of lymphocyte subsets.

INTRODUCTION

Immunity is tightly regulated to optimize protective responses against pathogens and malignancy while preventing inappropriate responses to otherwise benign antigens. Monogenic defects that impair this regulation of inflammation or tolerance result in a subgroup of the inborn errors of immunity (IEI) called primary immune regulatory disorders (PIRD)[1]. In contrast to classic IEIs, which typically manifest as unusually severe or recurrent infections, PIRDs predominantly present with immune-mediated pathology, including autoimmunity, lymphoproliferation, malignancy, autoinflammation, and atopy, with susceptibility to infections being a less pronounced aspect of these disorders[2].

Immune dysregulation can lead to a variety of hematologic manifestations and cytopenias[3]. A classic example is autoimmune hemolytic anemia (AIHA) caused by immune-mediated destruction of erythrocytes[4]. AIHA can be idiopathic (primary) or secondary and is classified as warm or cold (cold agglutinin disease [CAD], paroxysmal cold hemoglobinuria) depending on autoantibody behaviour at different thermal ranges, which is important for determining appropriate treatment regimens[5]. Most cases of AIHA are considered idiopathic (~60%)[6], while secondary causes can include IEIs/PIRDs, malignancy, bacterial/viral infections, and drugs[4]. As such, the etiology and pathogenesis of AIHA remains incompletely understood.

In the past 2 years, human germline variants in a family of transcription factors called the IKAROS zinc finger (IKZF) family have been linked to immunodeficiency and cytopenias[7-10]. Notably, loss-of-function (LOF) variants in *IKZF2* (Helios) were recently associated with combined immunodeficiency (CID) and/or immune dysregulation, including immune thrombocytopenia (ITP), Evan's syndrome, and systemic lupus erythematosus[7-9]. *IKZF2* is highly expressed in hematopoietic stem/progenitor cells, T cells, including activated $CD4^+$/$CD8^+$ T cells, mucosa-associated invariant T (MAIT) cells, regulatory T cells (Tregs), and natural killer (NK) cells[11-16]. As Tregs are among the highest *IKZF2* expressors, most studies have focused on the role of Helios in Treg development and function[17-27]. In mice, Helios is critical for Treg identity, survival, and stability, but is seemingly dispensable in mice and humans for suppressive function[20,27].

Nevertheless, both *IKZF2*$^{-/-}$ and Treg-specific *IKZF2*$^{-/-}$ mice develop progressive autoimmune disease associated with activated CD4^{+}/CD8^{+} T cells, increased T follicular helper (T_{FH}) and germinal center (GC) B cell numbers, autoantibody production, and increased proinflammatory cytokine production[19,20,28]. The role of *IKZF2* in other components of the human immune system (e.g. NK cells) is beginning to be better defined through the identification of humans with germline *IKZF2* variants[7-10].

Here, we report a detailed immunological and mechanistic workup of the first reported case of germline heterozygous dominant negative (DN) *IKZF2* disorder in a young girl we recently described[10]. This patient was found to have a novel genetic syndrome comprising Immunodysregulation, Craniofacial anomalies, Hearing impairment, Athelia, and Developmental delay (or ICHAD syndrome). We report a comprehensive mechanistic immune evaluation of this patient which revealed significant developmental and functional defects in NK and naïve CD4^{+} T cells and marked immune activation as the likely cause of immune dysregulation. Informed by our improved appreciation of the human phenotype caused by germline IKZF2 variants, we suggest that germline heterozygous dominant negative *IKZF2* variants should now be considered in the differential diagnosis of patients with AIHA and PIRD.

METHODS

Study participants and consent

All study participants and/or their parents/guardians provided written informed consent. Research study protocols (H18-02853, H18-02912, H15-00092) were approved by The University of British Columbia Clinical Research Ethics Board.

Cell isolation, culture, and immortalization

Peripheral blood mononuclear cells (PBMCs) were isolated from all study participants by standard Ficoll-Paque (GE Healthcare) density centrifugation as previously described[29]. Lymphoblastoid cell lines (LCLs) were derived by standard EBV transformation as previously described[29] (**Supplement**).

Plasmid generation and cloning

WT *IZKF2*, p.Gly136_Ser191dup *IKZF2*, pIL2-Luc2 plasmids were generated by introducing restriction sites into cDNA or genomic DNA by PCR and cloning into pCMV6-XL4-3xFLAG and p.GL4.14 firefly luciferase gene reporter (Promega) vectors, respectively (**Supplement**).

Transient transfections

HEK293 cells were transfected with empty vector (EV), WT, p.Gly136_Ser191dup, or varying ratios of WT/p.Gly136_Ser191dup *IKZF2* expression plasmids by Lipofectamine 3000 (ThermoFisher) transfection (**Supplement**). Transfected cells were then processed for immunoblotting or immunofluorescence. For luciferase assays, cells were additionally transfected with pIL2-Luc2 and Renilla luciferase (R-Luc) plasmids then processed with a Dual-Glo Luciferase Assay Kit (#E2920, Promega) (**Supplement**).

Immunoblotting

Helios protein detection was accomplished in LCLs and transfected HEK293 cells by standard immunoblotting as previously described[29] (**Supplement**).

Immunofluorescence

12mm coverslips were sterilized, HEK293 cells were seeded on top in 6-well plates, allowed to attach for 24h, then transfected as above. Transfected cells were fixed,

permeabilized, and stained for Helios, DAPI, and F-actin before mounting and imaging on a Leica SP5 II Laser Scanning Confocal Microscope (Leica Microsystems GmbH) (**Supplement**).

Immunophenotyping

Immunophenotyping and intracellular cytokine was performed as previously described[30]. Briefly, PBMCs were stimulated with PMA and ionomycin (P/I) in the presence of GolgiStop (#554724, BD Biosciences), stained with antibody panels 1-4 (**Supplemental Table 5**) using the eBioscience Foxp3 Transcription Factor Staining Buffer Set (#00-5523-00, Invitrogen, ThermoFisher), acquired on a FACSymphony flow cytometer, and analyzed using FlowJo (both BD Biosciences) (**Supplement**).

Proliferation assays

PBMCs were seeded at varying concentrations, labelled with Cell Proliferation Dye (CPD) eF450 (#65-0842-85, Invitrogen, ThermoFisher) and stimulated with anti-CD3/CD28-coated Dynabeads (#11141D, Human T-Expander, Gibco, ThermoFisher) for four days. Cells were stained with antibody panel 6 (**Supplemental Table 5**) and acquired on a CytoFLEX (Beckman Coulter) and analyzed using FlowJo (**Supplement**).

T cell suppression assays

Treg suppression of $CD3^+$ T cell proliferation was assessed as previously described[27]. Briefly, patient and control PBMCs were enriched for $CD4^+$ T cells, sorted using panel 7 (**Supplemental Table 5**) for Tregs and Tconvs, expanded with IL-2 and irradiated mouse L cells for seven days, then cocultured with various ratios of CPD-labelled anti-CD3/CD28 Dynabead-stimulated enriched $CD3^+$ T responder (Tresp) cells for four days. Percent suppression of $CD4^+$ and $CD8^+$ T cell proliferation was calculated using division index (DI): (1 - [DI of sample/DI of positive control]) x 100% (**Supplement**).

Quantification of cytokine production

Supernatants were collected from PBMCs stimulated for proliferation, cocultured Tregs and Tresp for T cell suppression assays, and stimulated Tregs and Tconvs alone. Cytokine concentrations were measured by LEGENDplex Human Th Cytokine Panel 12-plex (#741027, BioLegend) on a CytoFLEX (Beckman Coulter) and analyzed with

Qognit software (BioLegend) according to manufacturer's recommendations (**Supplement**).

TSDR methylation

Genomic DNA was isolated from expanded Tregs and Tconvs, bisulfite converted with an EZ DNA Methylation-Direct Kit (Zymo Research), PCR amplified, and pyrosequenced using a PyroMark Q96 MD (Qiagen) as previously described[27] (**Supplement**).

Single-cell RNA sequencing

Single-cell RNA sequencing was performed on unstimulated and 4h P/I-stimulated sorted Tregs and Tconv from P1 and two age-matched/sex-matched controls using the BD Rhapsody Single Cell platform (BD Biosciences) according to manufacturer's recommendations and analyzed as previously described[30] (**Supplement**). Raw data are deposited on Gene Expression Omnibus.

RESULTS

Clinical case presentation

The index patient (P1) is a 5-10-year-old girl born to non-consanguineous parents (**Figure 1A**) who presented with syndromic features of developmental abnormalities and immune dysregulation. Family history is unremarkable. She has profound bilateral sensorineural hearing loss, microcephaly, mild developmental delay, cleft palate, hypotonia, athelia, and dysmorphic facies (detailed in[10]). Consistent with underlying immune dysregulation, she has suffered from chronic anemia beginning at two months of age, which at times required hospitalization and red blood cell transfusions (**Figure 1B-I**). She also had severe atopic dermatitis beginning at ten months of age affecting the face, arms, legs, and trunk. Her skin inflammation was initially refractory to optimal medical therapy (i.e. topical corticosteroids, emollients, bleach baths), but has become more manageable with age. The patient also experienced frequent upper respiratory tract infections, which reduced in frequency following initiation of monthly intravenous immunoglobulin (IVIG) replacement therapy. Laboratory and hematologic evaluation revealed chronically positive direct antiglobulin tests (DAT) initially consistent with a mixed (cold>warm) AIHA phenotype, which progressed to a predominantly warm AIHA phenotype with age without overt hemolysis. Other notable hematological features included a normocellular bone marrow with scattered hemophagocytic macrophages, no morphological evidence for dysplastic cells or a progressive marrow disorder, lymphopenia, and elevated IgE (**Table 1**). Red cells did not carry any hemoglobin variants, although non-specific poikilocytosis and rouleaux formation were noted.

Given the unique constellation of features, P1 underwent trio WGS (detailed in[10]). This revealed a novel *de novo* germline heterozygous structural variant affecting *IKAROS zinc finger 2* (*IKZF2*) encoding Helios (NM_016260.3:c.406+540_574+13477dup; NP_057344.2:p.Gly136_Ser191dup) (**Figure 1J-K**). The variant results in intron 5 at chr2:213900960 being joined to intron 6 chr2:213921017 (GRCh37) with a 2 bp GT insertion in between. This leads to tandem duplication of exon 5 (~20kb duplication spanning exon 5 and parts of flanking introns), corresponding to tandem duplication of zinc fingers 2 and 3 of Helios (**Figure 1K**).

Characterization of the impact of the p.Gly136_Ser191dup Helios variant on protein expression and localization

The p.Gly136_Ser191dup Helios variant created a higher molecular weight Helios protein (as anticipated with a ~13kDa 56 amino acid duplication) detected in both transfected HEK293 cells and primary patient-derived LCLs (**Figure 2A, C** and detailed in[10]). Total Helios protein expression was reduced overall in both transfected HEK293 (**Figure 2A-B**) and patient-derived LCLs (**Figure 2C-E**), likely because the variant protein was less stable. As a TF, Helios localizes to the nucleus to regulate transcription[12]. We transfected HEK293 cells with WT or p.Gly136_Ser191dup *IKZF2* alone, or increasing quantities of p.Gly136_Ser191dup together with WT *IKZF2* (**Figure 2F**) to assess protein expression by immunofluorescence. The variant protein was indistinguishable from WT protein in nuclear localization, nor did it affect the nuclear localization of WT protein.

p.Gly136_Val192dup Helios acts through dominant interference

Helios has previously been shown to bind the *IL2* promoter to silence IL-2 production in Tregs[32]. We therefore cloned the human *IL2* promoter (-580 bp to +57 bp) into a firefly luciferase gene reporter vector and cotransfected this with Renilla luciferase, WT or p.Gly136_Ser191dup *IKZF2* alone, or p.Gly136_Ser191dup together with WT (**Figure 2G** and detailed in[10]). As expected, WT *IKZF2* strongly repressed *IL2* promoter activity. However, p.Gly136_Val192dup not only showed impaired repression on its own, but significantly interfered with WT *IKZF2*-mediated *IL2* repression (**Figure 2G**). This DN effect was dose-dependent, with increasing quantities of p.Gly136_Ser191dup transfected correlating with more impaired WT *IKZF2*-dependent *IL2* repression (r^2=0.94, p<0.0005) (**Figure 2H** and detailed in[10]).

Patient lymphocyte phenotyping reveals NK cell lymphocytosis and $CD3^+$ T cell lymphopenia

Helios is highly expressed in $CD3^+$ T cells and NK cells[11], both of which are known to be dysregulated in AIHA[4]. We profiled the frequencies of $CD3^+$ T, $CD3^-CD56^+$ NK, and $CD3^+CD56^+$ NKT cells as well as Helios expression from P1 (n=5 independent blood draws) and a cohort of adult (n=8) and age-matched controls (n=11). P1 had

significantly reduced frequencies of $CD3^+$ T (**Figure 3A-B**), markedly elevated NK (**Figure 3A,C**), and modestly elevated NKT (**Figure 3A,D**) cells, all of which were Helios-deficient (**Figure 3E-H**).

P1 NK cells are phenotypically immature and functionally abnormal

Given the intriguing NK cell lymphocytosis, we set out to define the developmental and functional status of P1 NK cells by assessing the expression of CD56, maturation (CD27, CD57, CD94), adhesion (CD16), and activation (CD8, CD25) markers[33-35] on P1 NK cells compared to controls. The relative abundance of $CD56^{dim}$ and $CD56^{bright}$ NK cell populations was normal (**Figure 3I-J**), although on histograms, the patient lacked a clear $CD56^{bright}$ population (**Figure S1A**). Strikingly, all maturation markers assessed were dysregulated in P1, including significantly reduced $CD16^+$ (**Figure 3K**, **Figure S1B**) and $CD57^+$ (**Figure 3L**, **Figure S1C**), but elevated $CD27^+$ (**Figure 3M**, **Figure S1D**) and $CD94^+$ (**Figure 3N**, **Figure S1E**) NK cells. Similarly, the frequency of $CD8^+$ NK cells were significantly reduced in the patient both at baseline and in response to stimulation (**Figure 3O**, **Figure S1F**), while $CD25^+$ NK cells (**Figure 3P**, **Figure S1G**) were normal. This abnormal distribution of markers disproportionately affected $CD56^{dim}$ NK cells more than $CD56^{bright}$ NK cells, although Helios was reduced in both populations (**Figure S1H-N**). Taken together, patient NK cells are skewed towards an immature phenotype.

As NK cells mediate their effector functions through the release of proinflammatory cytokines and cytolysis[33], we studied whether these roles were affected in P1. In response to stimulation, P1 had significantly elevated IFN-γ^+ NK cells (**Figure 3Q**, **Figure S1O**), but comparable TNF-α^+ NK cells (**Figure 3R**, **Figure S1P**). Similarly, P1 NK cells expressed significantly less granzyme B (**Figure 3S**) and perforin (**Figure 3T**), with this effect being more pronounced in $CD56^{dim}$ NK cells (**Figure S1Q-R**). These defects were confirmed in multidimensional space when we clustered live $CD3^-CD56^+$ NK cells from P1 and adult and pediatric controls on CD16, CD27, CD57, CD94, Helios, perforin, granzyme B, IFN-γ, and TNF-α at baseline and in response to stimulation (**Figure 3U-V**, **Figure S1S**).

Patient CD8$^+$ T cells are significantly reduced, have high PD-1 expression, and are potent proinflammatory cytokine producers

As CD8$^+$ T cells are frequently enriched in autoimmune disease[36] and can be clonally expanded in AIHA[37], we assessed the frequency of CD8$^+$ T cells and subsets and their Helios expression. P1 had profound CD8$^+$ T cell lymphopenia (**Figure 4A-B**), significantly elevated frequencies of central memory (CM) with a concurrent reduction in naïve subsets, while effector memory (EM) and TEMRA subsets were normal (**Figure 4C-G**). Importantly, all P1 CD8$^+$ T cell subsets were Helios-deficient (**Figure 4H-I**).

PD-1 is a critical inhibitory receptor that is upregulated in activated, memory, or exhausted T cells to restrain effector functions[38]. We therefore assessed PD-1 expression and proinflammatory cytokine production in P1 CD8$^+$ T cells. In line with elevated CD8 CM, we discovered significantly more PD-1 expression on P1 CD8$^+$ T cells (**Figure 4J-K**). These T cells are likely not exhausted as both naïve and total memory CD8$^+$ T cells produced significantly more TNF-α (**Figure 4L-N**) and IFN-γ (**Figure 4O-Q**) than controls, while CD8$^+$ T cell proliferation was comparable to controls (**Figure 4R-S**).

P1 CD19$^+$ B cells show largely normal development but increased TNF-α production

Although Ikaros and Aiolos are both critical for B cell differentiation[39], the role of Helios in these cells is less clear. Helios silencing is thought to maintain B cell function as ectopic expression leads to B cell hyperresponsiveness and lymphomagenesis[40]. We therefore studied the development and function of P1 B cells. In general, B cell development was largely normal, with intact total CD19$^+$ (**Figure S2A-B**), naïve (**Figure S2C, D**), switched memory [SM] (**Figure S2C, F**), and plasmablasts (**Figure S2I-J**). However, we did observe significantly increased non-switched memory [NSM] (**Figure S2C, E**) and decreased transitional B cells (**Figure S2G-H**), while Helios was lowly expressed in all B cell populations from both P1 and controls (**Figure S2K-L**). In response to stimulation, patient B cells produced significantly more TNF-α than controls (**Figure S2M**). This applied to NSM (**Figure S2N**), SM (**Figure S2O**), and naïve (**Figure S2P**) subsets.

P1 CD4$^+$ T cells are more mature

CD4$^+$ T helper (T_H) cells and their subsets are critical for both protective antimicrobial immunity and driving pathological states such as autoimmunity and atopic disease[41]. We therefore enumerated the frequency of total CD4$^+$ T cells and subsets and Helios expression. P1 CD4$^+$ T cells were modestly elevated (**Figure 5A**) in line with CD8$^+$ T lymphopenia. We also found similar subset distributions to P1 CD8$^+$ T cells, including significantly increased CD4$^+$ CM (**Figure 5B, D**), with an associated reduction in naïve (**Figure 5B, C**), while EM and TEMRA subsets (**Figure 5E-F**) were normal. Helios expression was low in all CD4$^+$ subsets (**Figure 5G-H**).

P1 CD4$^+$ T cells are hyperresponsive and exhibit effector phenotypes

In mice, Treg-specific, but not complete knockout, of *Ikzf2* in mice leads to increased PD-1 expression on CD4$^+$ T cells[20]. Surprisingly, P1 had three-fold higher PD-1$^+$ CD4$^+$ T cells than controls (**Figure 5I-J**), which could signify higher activation status. We thus measured the frequency of T_H subsets and cytokine production. Mirroring our *IL2* promoter luciferase data (**Figure 2F-G**), we observed a striking increase in IL-2$^+$ CD4$^+$ T cells in P1 (**Figure 5K-L**). This was not limited to IL-2, as the patient also had significantly increased IFN-γ^+ and TNF-α^+ CD4$^+$ T cells (**Figure 5M-P**) and most T_H subsets, including T_H1, T_H2 (**Figure 5Q-S**), T_H9, T_{FH} (**Figure 5T-V**), and T_H17 (**Figure S3A-B**). This also held true when we measured T_H cytokines in the supernatant of stimulated PBMCs, where we found markedly elevated concentrations of IL-2, IL-4, IL-5, IL-6, IL-9, IL-13, and TNF-α, even in response to lower bead:cell ratios (**Figure 5W, Figure S3C-N**). Surprisingly, we observed marked impairment in secreted IL-22 levels (**Figure S3L**). In keeping with this picture of hyperactive CD4$^+$ T cells, P1 CD4$^+$ T cells more readily proliferated in response to stimulation than controls (97.1% divided in patient vs. 54.5% in control) (**Figure 5X-Y**).

P1 has normal Treg frequencies and TSDR methylation

~70-80% of Tregs express Helios and at least in mice, this is thought to be important for regulating Treg identity and function[42]. As Tregs are critical mediators of tolerance/homeostasis and their dysfunction is associated with allergic and autoimmune disease[43], we enumerated their frequency and Helios expression in P1. P1 had normal

frequencies of $CD3^+CD4^+CD8^-CD25^+CD127^{lo}FOXP3^+$ Tregs (**Figure 6A, Figure S4A**), but significantly reduced Helios expression (**Figure 6B-C**).

Since methylation of the Treg-specific demethylated region (TSDR) in the *FOXP3* gene is important for maintaining stable FOXP3 expression and Treg suppressive function[44,45], we quantified expanded P1 Treg TSDR methylation and FOXP3 expression in comparison to Tregs from healthy female controls. TSDR methylation was normal (**Figure 6D**), although the average methylation trended to higher in P1 (**Figure S4B**). E*x vivo* P1 Tregs had significantly higher FOXP3 expression than controls, likely reflecting a higher state of activation (**Figure 6E**).

P1 Tregs are predominantly PD-1^+ and are potent T_H cytokine producers

Given the striking increase in PD-1^+ CD4+ (**Figure 5I-J**) and $CD8^+$ (**Figure 4J-K**) T cells in P1, we assessed PD-1 expression in P1 *ex vivo* Tregs. Similarly, P1 had significantly more PD-1^+ Tregs (~80%) than controls (~40%) (**Figure 6F, Figure S4C**). Helios genetic or pharmacological targeting in Tregs leads to elevated IL-2[32], IFN-γ, and IL-17A[19,20,28,46] and effector T_H cell signatures[47]. We thus studied T_H cytokine production in *ex vivo* Tregs and discovered significantly elevated IL-2^+ Tregs in P1 **(Figure 6G-H)**, confirming our *IL2* luciferase data (**Figure 2F-G**). P1 also had a striking increase in IL-4^+ (**Figure 6I-J**), IFN-γ^+ (**Figure 6I, K**), IL-9^+ (**Figure 6L, Figure S4D**), IL-21^+ **(Figure 6M, Figure S4D**), and TNF-α^+ (**Figure 6N-O**) Tregs. Expanded P1 Tregs also produced higher concentrations of IL-4, IL-5, IL-6, IL-9, IL-10, IL-13, and IL-17F (**Figure 6P, Figure S4C-N**).

P1 Tregs have impaired suppressive function are not intrinsically resistant to being suppressed

The abnormal cytokine production in P1 Tregs prompted us to investigate their ability to suppress T responder (Tresp) proliferation and cytokine production. We cocultured expanded P1 and control Tregs at different ratios with stimulated control $CD3^+$ Tresp. We discovered no significant differences between patient or control Treg-mediated suppression of $CD4^+$ (**Figure 6Q**) or $CD8^+$ (**Figure 6R**) T cell proliferation, although suppression trended to lower in the 1:2.5 and 1:5 Treg:CD3 T cell ratios.

An intrinsic resistance to Treg-mediated suppression could also contribute to the patient's prominent hyperactivation phenotype. We reversed our setup from above and cocultured control Tregs with P1 $CD3^+$ Tresp and measured suppression of T_H cytokines. P1 T_H cytokine production was effectively suppressed by control Tregs (**Figure 6S, Figure S5**), excluding an intrinsic defect in susceptibility to suppression.

scRNA-seq reveals a predominantly memory and effector phenotype in P1 Tregs

To assess transcriptomic pathways that could drive the striking patient Treg phenotype, we sorted $CD4^+CD25^+CD127^{lo}$ Tregs from P1 and two age-matched/sex-matched controls (**Figure S6A**). We carried out whole transcriptome single-cell RNA sequencing (scRNA-seq) on Tregs from P1 (n=295 cells) and controls (n=331 cells) and performed dimensionality reduction using the uniform manifold approximation and projection (UMAP) method[48]. Patient Tregs clustered separately from controls (**Figure 7A**) and when cell identity was annotated using the DICE project[49], they were predominantly labelled as memory Treg and T_H subsets (T_H1 T_H2, T_H17, T_{FH}), in line with the activated and aberrant cytokine phenotype observed (**Figure 6F-P**). Similarly, annotation based on CD45RA AbSeq/HLA-DR AbSeq expression to identify $CD45RA^+$HLA-DR^- naïve, $CD45RA^-$HLA-DR^+ activated, and $CD45RA^-$HLA-DR^- Tregs[50,51] also found that P1 Tregs were predominantly $CD45RA^-$HLA-DR^+ and $CD45RA^-$HLA-DR^-. (**Figure 7B**). Nevertheless, P1 Treg subsets were transcriptomically similar to control Tregs (**Figure 7C-E**, **Figure S6B-D**), except for significantly increased *IL2*, *PDCD1*, and *CCR4* transcript abundance in P1 naïve Tregs (**Figure 7C**), consistent with our flow cytometry data (**Figure 6F-H**).

scRNA-seq reveals a predominantly memory and effector phenotype in P1 $CD4^+$ Tconvs

Given the profound CD4 phenotype, we also sorted $CD4^+CD25^-CD127^+$ Tconv cells from P1 and two age-matched/sex-matched controls and performed scRNA-seq (P1 n=854 cells; control n=1225 cells) (**Figure S7A**). Like Tregs, P1 Tconv clustered separately from controls and were frequently labelled as T_H subsets (**Figure 7F**) and $CD45RA^-$ memory (**Figure 7G**). When comparing the transcriptome of AbSeq-inferred naïve (**Figure 7H, Figure S7E**) and memory (**Figure 7I, Figure S7F**) $CD4^+$ Tconv cells

between P1 and controls, we found similar memory, but distinctly different naïve populations. Unstimulated naïve P1 $CD4^+$ Tconv cells had significantly higher transcript abundance of genes related to IL-2 signalling, activation, and migration (*IL2RB*, *CXCR4*, *PDCD1*, *CCL5*, *JUN*). Stimulated P1 $CD4^+$ Tconv cells had significantly higher expression of proinflammatory cytokine/chemokine genes (*IL2*, *IFNG*, *TNF*, *CCL4*), confirming our $CD4^+$ phenotyping data (**Figure 5K-P**).

P1 $CD4^+$ Tconvs are poised for T_H differentiation

To study what pathways could be driving naïve $CD4^+$ Tconv differences, we carried out gene set enrichment analyses. Unstimulated naïve P1 $CD4^+$ Tconv cells were more enriched in pathways related to proliferation, IL-6 signalling, allograft rejection, apoptosis, and hypoxia. Further, stimulated patient $CD4^+$ Tconv cells showed significant enrichment in proliferation (Myc targets V1/V2), metabolism (glycolysis, gluconeogenesis, mTORC1 signaling), Treg survival (IL-2-STAT5), impaired tolerance (allograft rejection), atopy (TSLP pathway), and T_H differentiation (IL-27-/IL-12-/IL-23-mediated signalling events, T_H1, T_H2, T_H17 cell differentiation) pathways (**Figure 7J**). In line with the primed/poised phenotype of P1 naïve $CD4^+$ Tconv cells, we observed significantly increased IL-2^+ (**Figure 7K-L**), IFN-γ^+ (**Figure 7M-N**), and TNF-α^+ (**Figure 7O-P**) naïve P1 $CD4^+$ T cells, with a similar trend observed in memory.

DISCUSSION

Germline pathogenic variants in *IKZF2* have only been discovered in humans in the past two years. The initial descriptions were of germline heterozygous or homozygous LOF *IKZF2* variants in a total of 13 patients with combined immunodeficiency and/or immune dysregulation[7-9] (summarized in **Figure S7A, Table S3**). Collectively, these germline LOF *IKZF2* variants were predominantly heterozygous (10/13) and were mostly associated with evidence of immune dysregulation (10/13) (**Table S4**), including systemic lupus erythematosus (SLE), hemophagocytic lymphohistiocytosis (HLH), idiopathic thrombocytopenic purpura (ITP), and Evan's syndrome. Our group recently expanded this list through the discovery of 2 patients with germline DN *IKZF2* variants who presented with ICHAD syndrome[10]. Notably the patient carrying the DN pathogenic c.406+540_574+13477dup;p.Gly136_Ser191dup *IKZF2* variant (designated P1) experienced the most severe clinical manifestations of immune dysregulation out of all 15 patients described to date with pathogenic germline *IKZF2* variants (**Figure S7B**). P1 presented with syndromic developmental features plus significant chronic AIHA and atopic dermatitis, features consistent with classification as a PIRD. Given the profound immune dysregulation associated with the DN pathogenic c.406+540_574+13477dup;p.Gly136_Ser191dup *IKZF2* variant, we embarked on a detailed immunological assessment of P1.

Immunophenotyping of this patient with DN *IKZF2* deficiency revealed striking differences from previous homozygous and heterozygous LOF patients and mice. For example, P1 NK cells were phenotypically immature and likely hyperactive due to elevated IFN-γ production and reduced intracellular perforin and granzyme B expression (**Figure 3**). In contrast, other reported patients had NK cell lymphopenia[8,9] or normal NK development[7]. Furthermore, while *IKZF2*$^{-/-}$ mice have normal NK cell frequencies[21], NK cells from NKp46-mutant mice (Noé) show elevated Helios expression and effector function, which modulates protective memory CD4^{+}/CD8^{+} T cell development[52]. The study of P1 has thus revealed a previously unappreciated role for Helios in human NK cell development and function and calls for more in-depth studies in the future.

Helios has been extensively studied in mouse Tregs[42], but its role in human Tregs has remained relatively unclear. Previous CRISPR-mediated KO studies by our co-authors found that Helios is dispensable for lineage stability and suppressive function in fully differentiated Tregs[27], whereas germline homozygous or heterozygous LOF *IKZF2* variants caused a proinflammatory Treg phenotype associated with increased IL-2 and IFN-γ production, but intact suppressive function[7,8]. Our functional studies with this DN *IKZF2* variant confirm that it is not required for Treg development, but that it is essential for inhibition of IL-2 expression and many other cytokines. Although functional suppression of T cell proliferation appeared normal, aberrant production of many T_H cytokines likely contributes to a functional defect in immune regulation *in vivo* (**Figure 6**), which is exacerbated by the greater propensity of P1 naïve $CD4^+$ T cells to differentiate into effector $CD4^+$ T cell subsets (T_H1, T_H2, T_H9, T_{FH}).

Taken together, we have defined the immune phenotype of a novel form of Helios deficiency caused by a DN variant, which leads to severe congenital AIHA and atopic dermatitis[10]. This study identifies new players in the pathogenesis of these immune-mediated disorders and has significantly expanded our understanding of human Helios, including its regulation of naïve CD4 T cell differentiation into memory/effector subsets and NK cell development and function.

ACKNOWLEDGEMENTS

This work was supported in part by grants from the Canadian Institutes of Health Research (PJT 178054 to S.E.T.; FDN-154304 to M.K.L.), Genome British Columbia (SIP007) (S.E.T.), and BC Children's Hospital Foundation. S.E.T. holds a Tier 1 Canada Research Chair in Pediatric Precision Health and the Aubrey J. Tingle Professor of Pediatric Immunology. M.K.L. receives a BCCHR salary award and holds a Tier 1 Canada Research Chair in Engineered Immune Tolerance. H.Y.L. is supported by a CIHR Frederick Banting and Charles Best Canada Graduate Scholarships Doctoral Award (CGS-D), University of British Columbia Four Year Doctoral Fellowship (4YF), Killam Doctoral Scholarship, Friedman Award for Scholars in Health, and a BC Children's Hospital Research Institute Graduate Studentship. M.V.S. is supported by a Vanier Canada Graduate Scholarship and 4YF. A.J.L. is supported by a CGS-D and 4YF. M.S. is supported by a CGS-D and 4YF. We would like to acknowledge the Flow Cytometry and Imaging cores at BC Children's Hospital Research Institute for providing the equipment for microscopy, flow cytometry, and cell sorting, the Biomedical Research Centre Sequencing Core (BRC-Seq) for their assistance with single-cell RNA sequencing and data processing, The Centre for Applied Genomics, The Hospital for Sick Children, Toronto, Canada for their assistance with whole genome sequencing, and the BC Children's Hospital BioBank for providing access to age-matched and sex-matched control peripheral blood mononuclear cells.

AUTHORSHIP CONTRIBUTIONS

H.Y.L, A.L., and S.E.T. were responsible for study conception and design. H.Y.L., M.V.S., A.J.L., M.S., J.G., G.X.Y., S.L. performed experiments. A.M., C.V., A.L., S.M. conducted genetic screening and variant prioritization. H.Y.L., M.S., M.P.F., M.S.K., A.M performed bioinformatics analyses or provided computational resources. H.Y.L., M.V.S., A.S., R.R., L.A., J.H., C.L.Y., M.C., E.H., Au.S., F.K.K., K.J.H., C.M.B., C.V., A.L., S.E.T. collected and analyzed clinical data. H.Y.L., M.V.S., A.J.L., M.S., A.M., J.G., G.X.Y., M.K.L., S.E.T. analyzed and interpreted data. H.Y.L. and S.E.T. wrote the manuscript with input from all authors. All authors read and approved the final version of the manuscript.

DISCLOSURE OF CONFLICTS OF INTEREST

The authors declare no competing financial interests.

REFERENCES

1. Chan AY, Torgerson TR. Primary immune regulatory disorders: a growing universe of immune dysregulation. *Curr Opin Allergy Clin Immunol*. 2020;20(6):582-590.
2. Flinn AM, Gennery AR. Primary immune regulatory disorders: Undiagnosed needles in the haystack? *Orphanet J Rare Dis*. 2022;17(1):99.
3. Seidel MG. Autoimmune and other cytopenias in primary immunodeficiencies: pathomechanisms, novel differential diagnoses, and treatment. *Blood*. 2014;124(15):2337-2344.
4. Michalak SS, Olewicz-Gawlik A, Rupa-Matysek J, Wolny-Rokicka E, Nowakowska E, Gil L. Autoimmune hemolytic anemia: current knowledge and perspectives. *Immun Ageing*. 2020;17(1):38.
5. Zanella A, Barcellini W. Treatment of autoimmune hemolytic anemias. *Haematologica*. 2014;99(10):1547-1554.
6. Tranekaer S, Hansen DL, Frederiksen H. Epidemiology of Secondary Warm Autoimmune Haemolytic Anaemia-A Systematic Review and Meta-Analysis. *J Clin Med*. 2021;10(6).
7. Hetemaki I, Kaustio M, Kinnunen M, et al. Loss-of-function mutation in IKZF2 leads to immunodeficiency with dysregulated germinal center reactions and reduction of MAIT cells. *Sci Immunol*. 2021;6(65):eabe3454.
8. Shahin T, Kuehn HS, Shoeb MR, et al. Germline biallelic mutation affecting the transcription factor Helios causes pleiotropic defects of immunity. *Sci Immunol*. 2021;6(65):eabe3981.
9. Shahin T, Mayr D, Shoeb MR, et al. Identification of germline monoallelic mutations in IKZF2 in patients with immune dysregulation. *Blood Adv*. 2022;6(7):2444-2451.
10. Mohajeri A, Vaseghi-Shanjani M, Rosenfeld JA, et al. Dominant negative variants in IKZF2 cause ICHAD syndrome, a new disorder characterised by immunodysregulation, craniofacial anomalies, hearing impairment, athelia and developmental delay. *J Med Genet*. 2023.
11. Kelley CM, Ikeda T, Koipally J, et al. Helios, a novel dimerization partner of Ikaros expressed in the earliest hematopoietic progenitors. *Curr Biol*. 1998;8(9):508-515.
12. Hahm K, Cobb BS, McCarty AS, et al. Helios, a T cell-restricted Ikaros family member that quantitatively associates with Ikaros at centromeric heterochromatin. *Genes Dev*. 1998;12(6):782-796.
13. Getnet D, Grosso JF, Goldberg MV, et al. A role for the transcription factor Helios in human CD4(+)CD25(+) regulatory T cells. *Mol Immunol*. 2010;47(7-8):1595-1600.
14. Akimova T, Beier UH, Wang L, Levine MH, Hancock WW. Helios expression is a marker of T cell activation and proliferation. *PLoS One*. 2011;6(8):e24226.
15. Serre K, Benezech C, Desanti G, et al. Helios is associated with CD4 T cells differentiating to T helper 2 and follicular helper T cells in vivo independently of Foxp3 expression. *PLoS One*. 2011;6(6):e20731.
16. Leeansyah E, Svard J, Dias J, et al. Arming of MAIT Cell Cytolytic Antimicrobial Activity Is Induced by IL-7 and Defective in HIV-1 Infection. *PLoS Pathog*. 2015;11(8):e1005072.

17. Thornton AM, Korty PE, Tran DQ, et al. Expression of Helios, an Ikaros transcription factor family member, differentiates thymic-derived from peripherally induced Foxp3+ T regulatory cells. *J Immunol*. 2010;184(7):3433-3441.
18. Thornton AM, Lu J, Korty PE, et al. Helios(+) and Helios(-) Treg subpopulations are phenotypically and functionally distinct and express dissimilar TCR repertoires. *Eur J Immunol*. 2019;49(3):398-412.
19. Kim HJ, Barnitz RA, Kreslavsky T, et al. Stable inhibitory activity of regulatory T cells requires the transcription factor Helios. *Science*. 2015;350(6258):334-339.
20. Sebastian M, Lopez-Ocasio M, Metidji A, Rieder SA, Shevach EM, Thornton AM. Helios Controls a Limited Subset of Regulatory T Cell Functions. *J Immunol*. 2016;196(1):144-155.
21. Cai Q, Dierich A, Oulad-Abdelghani M, Chan S, Kastner P. Helios deficiency has minimal impact on T cell development and function. *J Immunol*. 2009;183(4):2303-2311.
22. Ross EM, Bourges D, Hogan TV, Gleeson PA, van Driel IR. Helios defines T cells being driven to tolerance in the periphery and thymus. *Eur J Immunol*. 2014;44(7):2048-2058.
23. Skadow M, Penna VR, Galant-Swafford J, Shevach EM, Thornton AM. Helios Deficiency Predisposes the Differentiation of CD4(+)Foxp3(-) T Cells into Peripherally Derived Regulatory T Cells. *J Immunol*. 2019;203(2):370-378.
24. Himmel ME, MacDonald KG, Garcia RV, Steiner TS, Levings MK. Helios+ and Helios- cells coexist within the natural FOXP3+ T regulatory cell subset in humans. *J Immunol*. 2013;190(5):2001-2008.
25. Gottschalk RA, Corse E, Allison JP. Expression of Helios in peripherally induced Foxp3+ regulatory T cells. *J Immunol*. 2012;188(3):976-980.
26. Ng MSF, Roth TL, Mendoza VF, Marson A, Burt TD. Helios enhances the preferential differentiation of human fetal CD4(+) naive T cells into regulatory T cells. *Sci Immunol*. 2019;4(41).
27. Lam AJ, Uday P, Gillies JK, Levings MK. Helios is a marker, not a driver, of human Treg stability. *Eur J Immunol*. 2022;52(1):75-84.
28. Nakagawa H, Sido JM, Reyes EE, Kiers V, Cantor H, Kim HJ. Instability of Helios-deficient Tregs is associated with conversion to a T-effector phenotype and enhanced antitumor immunity. *Proc Natl Acad Sci U S A*. 2016;113(22):6248-6253.
29. Lu HY, Sharma M, Sharma AA, et al. Mechanistic understanding of the combined immunodeficiency in complete human CARD11 deficiency. *J Allergy Clin Immunol*. 2021;148(6):1559-1574 e1513.
30. Sharma M, Fu MP, Lu HY, et al. Human complete NFAT1 deficiency causes a triad of joint contractures, osteochondromas, and B cell malignancy. *Blood*. 2022.
31. Chessum L, Matern MS, Kelly MC, et al. Helios is a key transcriptional regulator of outer hair cell maturation. *Nature*. 2018;563(7733):696-700.
32. Baine I, Basu S, Ames R, Sellers RS, Macian F. Helios induces epigenetic silencing of IL2 gene expression in regulatory T cells. *J Immunol*. 2013;190(3):1008-1016.
33. Abel AM, Yang C, Thakar MS, Malarkannan S. Natural Killer Cells: Development, Maturation, and Clinical Utilization. *Front Immunol*. 2018;9:1869.
34. Burk CM, Coffey KE, Mace EM, et al. Immunodeficiency, centromeric instability, and facial anomalies (ICF) syndrome with NK dysfunction and EBV-driven malignancy

595 treated with stem cell transplantation. *J Allergy Clin Immunol Pract*. 2020;8(3):1103-
596 1106 e1103.
597 35. Ruiz-Garcia R, Vargas-Hernandez A, Chinn IK, et al. Mutations in PI3K110delta
598 cause impaired natural killer cell function partially rescued by rapamycin treatment. *J*
599 *Allergy Clin Immunol*. 2018;142(2):605-617 e607.
600 36. Petrelli A, Mijnheer G, Hoytema van Konijnenburg DP, et al. PD-1+CD8+ T cells
601 are clonally expanding effectors in human chronic inflammation. *J Clin Invest*.
602 2018;128(10):4669-4681.
603 37. Smirnova SJ, Sidorova JV, Tsvetaeva NV, et al. Expansion of CD8+ cells in
604 autoimmune hemolytic anemia. *Autoimmunity*. 2016;49(3):147-154.
605 38. Kuchroo JR, Hafler DA, Sharpe AH, Lucca LE. The double-edged sword:
606 Harnessing PD-1 blockade in tumor and autoimmunity. *Sci Immunol*.
607 2021;6(65):eabf4034.
608 39. Heizmann B, Kastner P, Chan S. The Ikaros family in lymphocyte development.
609 *Curr Opin Immunol*. 2018;51:14-23.
610 40. Dovat S, Montecino-Rodriguez E, Schuman V, Teitell MA, Dorshkind K, Smale
611 ST. Transgenic expression of Helios in B lineage cells alters B cell properties and
612 promotes lymphomagenesis. *J Immunol*. 2005;175(6):3508-3515.
613 41. Zhu X, Zhu J. CD4 T Helper Cell Subsets and Related Human Immunological
614 Disorders. *Int J Mol Sci*. 2020;21(21).
615 42. Thornton AM, Shevach EM. Helios: still behind the clouds. *Immunology*.
616 2019;158(3):161-170.
617 43. Sakaguchi S, Mikami N, Wing JB, Tanaka A, Ichiyama K, Ohkura N. Regulatory
618 T Cells and Human Disease. *Annu Rev Immunol*. 2020;38:541-566.
619 44. Floess S, Freyer J, Siewert C, et al. Epigenetic control of the foxp3 locus in
620 regulatory T cells. *PLoS Biol*. 2007;5(2):e38.
621 45. Polansky JK, Kretschmer K, Freyer J, et al. DNA methylation controls Foxp3
622 gene expression. *Eur J Immunol*. 2008;38(6):1654-1663.
623 46. Wang ES, Verano AL, Nowak RP, et al. Acute pharmacological degradation of
624 Helios destabilizes regulatory T cells. *Nat Chem Biol*. 2021;17(6):711-717.
625 47. Yates K, Bi K, Haining WN, Cantor H, Kim HJ. Comparative transcriptome
626 analysis reveals distinct genetic modules associated with Helios expression in
627 intratumoral regulatory T cells. *Proc Natl Acad Sci U S A*. 2018;115(9):2162-2167.
628 48. McInnes L, Healy J, Melville J. UMAP: Uniform Manifold Approximation and
629 Projection for Dimension Reduction; 2018:arXiv:1802.03426.
630 49. Schmiedel BJ, Singh D, Madrigal A, et al. Impact of Genetic Polymorphisms on
631 Human Immune Cell Gene Expression. *Cell*. 2018;175(6):1701-1715 e1716.
632 50. Dong S, Maiella S, Xhaard A, et al. Multiparameter single-cell profiling of human
633 CD4+FOXP3+ regulatory T-cell populations in homeostatic conditions and during graft-
634 versus-host disease. *Blood*. 2013;122(10):1802-1812.
635 51. Rosenblum MD, Way SS, Abbas AK. Regulatory T cell memory. *Nat Rev*
636 *Immunol*. 2016;16(2):90-101.
637 52. Narni-Mancinelli E, Jaeger BN, Bernat C, et al. Tuning of natural killer cell
638 reactivity by NKp46 and Helios calibrates T cell responses. *Science*.
639 2012;335(6066):344-348.
640

TABLE LEGENDS

Table 1. Summary of major hematological and immunological laboratory parameters. Tabulation of patient hematological and immunological laboratory values compared to age-specific reference ranges. ‡value measured while patient was on intravenous immunoglobulin replacement. TREC, T cell receptor excision circle; DAT, direct antiglobulin test; HGB, hemoglobin.

FIGURE LEGENDS

Figure 1. Clinical phenotype of the patient. A) Family pedigree of the patient. Filled symbols indicate affected individuals. Arrow represents index patient. Known genotype is marked. B-I) Hematological parameters measured in the patient over time. Shaded regions=age-specific reference ranges. J) Sanger sequencing of DNA extracted from whole blood of the patient. Primers were designed to flank the breakpoint. K) Schematic representation of the impact of i) the c.406+540_574+13477dup *IKZF2* variant on the genomic level. Red inset=exon 5 duplication. Blue inset=Sanger sequencing primer location; and ii) the p.Gly136_Ser191dup Helios variant on the protein level. Red inset=zinc finger 2 and 3 duplication. Var., variant; WT, wild-type; ZF, zinc finger; P1, patient 1.

Figure 2. A novel *IKZF2* variant leads to reduced Helios protein expression and dominant interference of WT function. A-B) HEK293 cells were transfected with empty vector (EV), wild-type (WT) *IKZF2*, or p.Gly136_Ser191dup (variant) *IKZF2* alone or in different combinations. Expression was determined by immunoblotting with both FLAG and Helios. n=5. C-E) Expression of Helios was detected in patient-derived and control lymphoblastoid cell lines (LCLs) and compared to negative (THP-1 monocytic cells) and positive (Jurkat T leukemia cells) controls by C-D) immunoblot and E) flow cytometry. F) HEK293 cells were transfected with EV, WT, variant, or ratios of WT:variant and subjected to immunofluorescence for detection of Helios (red, Alexa Fluor 647), the nucleus (blue, DAPI), and F-actin (green, Phalloidin Alexa Fluor 488) using a Leica SP5 Confocal and LAS X Software with a 100x objective lens. Scale

bars=5µm. n=3. G-H) HEK293 cells were cotransfected with EV, *IKZF2* expression plasmids at various ratios, pIL2-luc2, and Renilla luciferase. *IL2* promoter activity was defined as relative light units from different conditions normalized to EV. H) Pearson correlation between *IL2* promoter activity and % variant/WT *IKZF2* plasmid transfected. Shaded region=95% confidence interval. n=3. *p<0.05, **p<0.01, ***p<0.001, ****p<0.0001. Ordinary one-way ANOVA with Šidák's multiple comparisons test.

Figure 3. P1 has impaired NK cell development and function. A) Representative flow cytometry dot plots showing $CD3^+CD56^-$ T cells, $CD3^-CD56^+$ NK cells, and $CD3^+CD56^+$ NKT cells for P1 and a control. B-D) Frequency of B) T cells, C) NK cells, D) NKT cells from A) in P1 and adult (HC^A) and pediatric (HC^P) controls. E) Representative Helios histograms for T, NK, and NKT cells in P1 and controls compared to a fluorescence minus one (FMO) control. Mean fluorescence intensities (MFI) are indicated. F-H) Quantification of Helios MFI in F) T cells, G) NK cells, H) NKT cells from P1 and controls. I-N) Frequency of I) $CD56^{dim}$, J) $CD56^{bright}$ NK, K) $CD16^+$, L) $CD57^+$, M) $CD27^+$, N) $CD94^+$ NK cells in P1 compared to controls. O-P) Frequency of N) $CD8^+$ and P) $CD25^+$ NK cells in patient and controls before and after 4h PMA and ionomycin (P/I) stimulation. Q-R) Frequency of Q) IFN-γ^+ and R) TNF-α^+ NK cells in P1 and controls after P/I stimulation. S-T) MFI of S) granzyme B and T) perforin in unstimulated P1 and control NK cells. U-V) Live NK cells from P1 or controls clustered on CD16, CD27, CD57, CD94, Helios, perforin, granzyme B, IFN-γ, and TNF-α. Number of NK cells clustered for each group is indicated on the panels to the right. V) tSNE plots from U) coloured based on CD16, CD27, CD56, CD57, or CD94 expression. A-N, Q-T) P1 n=5, HC^A n=8, HC^P n=11. O-P) P1 n=3, HC n=8. *p<0.05, **p<0.01, ***p<0.001, ****p<0.0001. Ordinary one-way ANOVA with Šidák's multiple comparisons test.

Figure 4. P1 $CD8^+$ T cells are more differentiated and have enhanced cytokine production. A) Representative dot plots showing $CD3^+CD4^-CD8^+$ and $CD3^+CD4^+CD8^-$ T cells. B) Frequency of $CD8^+$ T cells in P1 and adult (HC^A) or pediatric (HC^P) controls. C) Representative contour plot of naïve (N), central memory (CM), effector memory (EM), and TEMRA $CD8^+$ T cells in the patient and a control. Quadrants corresponding to each subset are shown to the right. D-G) Quantification of D) naive, E) CM, F) EM, G)

TEMRA $CD8^+$ T cells from C). H) Representative Helios histograms for $CD8^+$ T cells from P1 and three controls compared to a fluorescence minus one (FMO) control. Mean fluorescence intensities (MFI) are indicated. I) Quantification of Helios MFI in different $CD8^+$ T cell subsets. J) Representative contour plots for PD-1^+ $CD8^+$ T cells in P1 and a control. K) Quantification of J). L-Q) PBMCs stimulated 4h with PMA+ionomycin. L), O) Representative contour plots for L) TNF-α^+ and O) IFN-γ^+ $CD8^+$ T cells in P1 and a control. M-N) Quantification of TNF-α^+ M) naïve and N) total memory $CD8^+$ T cells. P-Q) Quantification of IFN-γ^+ P) naïve and Q) total memory $CD8^+$ T cells. A-Q) P1 n=5, HC^A n=8, HC^P n=11. J-K) P1 n=3, HC^A n=8. *p<0.05, **p<0.01, ***p<0.001, ****p<0.0001. Ordinary one-way ANOVA with Šidák's multiple comparisons test. R) Representative histograms for dilution of Cell Proliferation Dye (CPD) eF450 in P1 or control $CD8^+$ T cells after 4 days of stimulation with anti-CD3/CD28 beads at 1:32 bead to cell ratio. S) Quantification of percent divided $CD8^+$ T cells at 1:8, 1:16, 1:32 bead to cell ratios. Shown are technical duplicates.

Figure 5. P1 $CD4^+$ T cells are hyperactive and exhibit enhanced effector function. A) Quantification of frequency of $CD4^+$ T cells in P1 and adult (HC^A) or pediatric (HC^P) controls. B) Representative contour plot of naïve (N), central memory (CM), effector memory (EM), and TEMRA $CD4^+$ T cells in the patient and a control. Quadrants corresponding to each subset are shown to the right. C-F) Quantification of C) naïve, D) CM, E) EM, F) TEMRA $CD4^+$ T cells from B). G) Representative Helios histograms for $CD4^+$ T cells in P1 and three controls compared to a fluorescence minus one (FMO) control. Mean fluorescence intensities (MFI) are indicated. H) Quantification of Helios MFI in different $CD4^+$ T cell subsets. I) Representative contour plots for PD-1^+ $CD4^+$ T cells in P1 and a control. J) Quantification of I). K-V) PBMCs stimulated 4h with PMA+ionomycin. K), M), O), Q), T) Representative contour plots for K) IL-2^+ $CD4^+$ M) IFN-γ^+ $CD4^+$, O) TNF-α^+ $CD4^+$, Q) IFN-γ^+IL-4^- T_H1 and IFN-γ^-IL-4^+ T_H2, T) IL-21^+IL-9^- T_{FH} and IL-21^-IL-9^+ T_H9 cells in P1 and a control. Quadrant identities are shown on the bottom right. Frequencies corresponding to each quadrant are included to the top right of each panel. L), N), P), R-S), U-V) Quantification of L) IL-2^+ $CD4^+$, N) IFN-γ^+ $CD4^+$, P) TNF-α^+ $CD4^+$, R) T_H1, S) T_H2), U) T_H9, V) T_{FH} cells. A-H), K-V) P1 n=5, HC^A n=8, HC^P

n=11. I-J) P1 n=3, HC^A n=8. *p<0.05, **p<0.01, ***p<0.001, ****p<0.0001. Ordinary one-way ANOVA with Šidák's multiple comparisons test. W-Y) PBMCs stimulated with anti-CD3/CD28 beads at various bead to cell ratios for 4 days. W) T_H cytokines measured by LEGENDplex. X) Representative histograms for dilution of Cell Proliferation Dye (CPD) eF450 in P1 or control $CD4^+$ T cells stimulated at 1:32 bead to cell ratio. Y) Quantification of percent divided $CD4^+$ T cells at 1:8, 1:16, 1:32 bead to cell ratios. Shown are technical duplicates.

Figure 6. P1 Tregs have aberrant cytokine production and impaired suppressive function. A) Quantification of frequency of $CD3^+CD4^+CD8^-CD25^+CD127^{lo}FOXP3^+$ Tregs in P1 and adult (HC^A) or pediatric (HC^P) controls. B) Representative Helios histograms for Tregs in P1 and three controls compared to a fluorescence minus one (FMO) control. Mean fluorescence intensities (MFI) are indicated. C) Quantification of Helios MFI in Tregs. D) CpG methylation of the Treg-specific demethylated region (TSDR) for P1 or control Tregs and Tconvs. Percent methylation at different TSDR CpG sites is indicated. Representative of n=2. E) Quantification of FOXP3 MFI in Tregs. F) Quantification of $PD\text{-}1^+$ Tregs. G-O) PBMCs stimulated 4h with PMA+ionomycin. G), I), N) Representative contour plots for G) $IL\text{-}2^+$, I) $IFN\text{-}\gamma^+$, $IL\text{-}4^+$, and N) $TNF\text{-}\alpha^+$ Tregs. H), J-M), O) Quantification of H) $IL\text{-}2^+$, J) $IL\text{-}4^+$, K) $IFN\text{-}\gamma^+$, L) $IL\text{-}9^+$, M) $IL\text{-}21^+$, O) $TNF\text{-}\alpha^+$ Tregs. A-C), E), J-O) P1 n=5, HC^A n= 10, HC^P n=12. F-H) P1 n=3, HC^A n=8. *p<0.05, **p<0.01, ***p<0.001, ****p<0.0001. Ordinary one-way ANOVA with Šidák's multiple comparisons test. P) Isolated and expanded Tregs stimulated with anti-CD3/CD28 beads for 4 days. T_H cytokines measured by LEGENDplex. Shown are 3 technical replicates. Q-R) Isolated and expanded Tregs co-cultured at different ratios with control $CD3^+$ T responder (Tresp) cells. n=2. Q-R) Suppression of Q) $CD4^+$ and R) $CD8^+$ T cell proliferation. Significance determined by one-way ANOVA of areas under the curve. S) T_H cytokines measured by LEGENDplex when co-culturing 1:16 bead:cell ratio stimulated P1 $CD3^+$ Tresp with control Tregs. Shown are technical triplicates.

Figure 7. P1 naïve $CD4^+$ T cells are more active and primed for effector function. A-E) Single-cell RNA sequencing (scRNA-seq) of sorted $CD3^+CD4^+CD25^+CD127^{lo}$ Tregs from P1 and 2 age-matched and sex-matched controls. A) Unstimulated Tregs

clustered and annotated using the DICE project and B) CD45RA/HLA-DR AbSeq labelling. Panels represent the controls and P1 Tregs clustered together (overall) or control or P1 Tregs alone. Included are legends with colours and numbers corresponding to each cell type labelled. Doughnut plots are included below each panel to represent the frequency of each annotated cell type. C-E) Volcano plots comparing stimulated patient and control C) $CD45RA^{+}HLA\text{-}DR^{-}$ naïve, D) $CD45RA^{-}HLA\text{-}DR^{+}$ activated, and E) $CD45RA^{-}HLA\text{-}DR^{-}$ Tregs. Red=significantly increased, blue=significantly decreased, gray=non-significant. Vertical dashed line: fold change=1.5, horizontal dashed line: FDR=0.05. Top 10 most significant genes are labelled. F-H) scRNA-seq of sorted $CD3^{+}CD4^{+}CD25^{-}CD127^{hi}$ Tconv from P1 and 2 age-matched and sex-matched controls. F-G) Unstimulated Tconv clustered and annotated as in A-B). H-I) Volcano plots as in C-E) comparing stimulated patient and control H) $CD45RA^{+}$ naïve or I) $CD45RA^{-}$ memory Tconvs. J) Gene set enrichment of differentially expressed genes between stimulated naïve patient and control Tconvs using EnrichR. Shown are the combined scores and adjusted p-values. H=MSigDB Hallmark, B=BioPlanet 2019, N=NCI Nature 2016, K=KEGG 2021 Human. K-P) PBMCs stimulated 4h with PMA+ionomycin. Quantification of stimulated K) IL-2^{+} naïve, L) IL-2^{+} total memory, M) IFN-γ^{+} naïve, N) IFN-γ^{+} total memory, O) TNF-α^{+} naïve, and P) TNF-α^{+} total memory $CD4^{+}$ T cells. K-P) P1 n=5, HC^{A} n=8, HC^{P} n=11. ***p<0.001, ****p<0.0001. Ordinary one-way ANOVA with Šidák's multiple comparisons test.

Figure 1

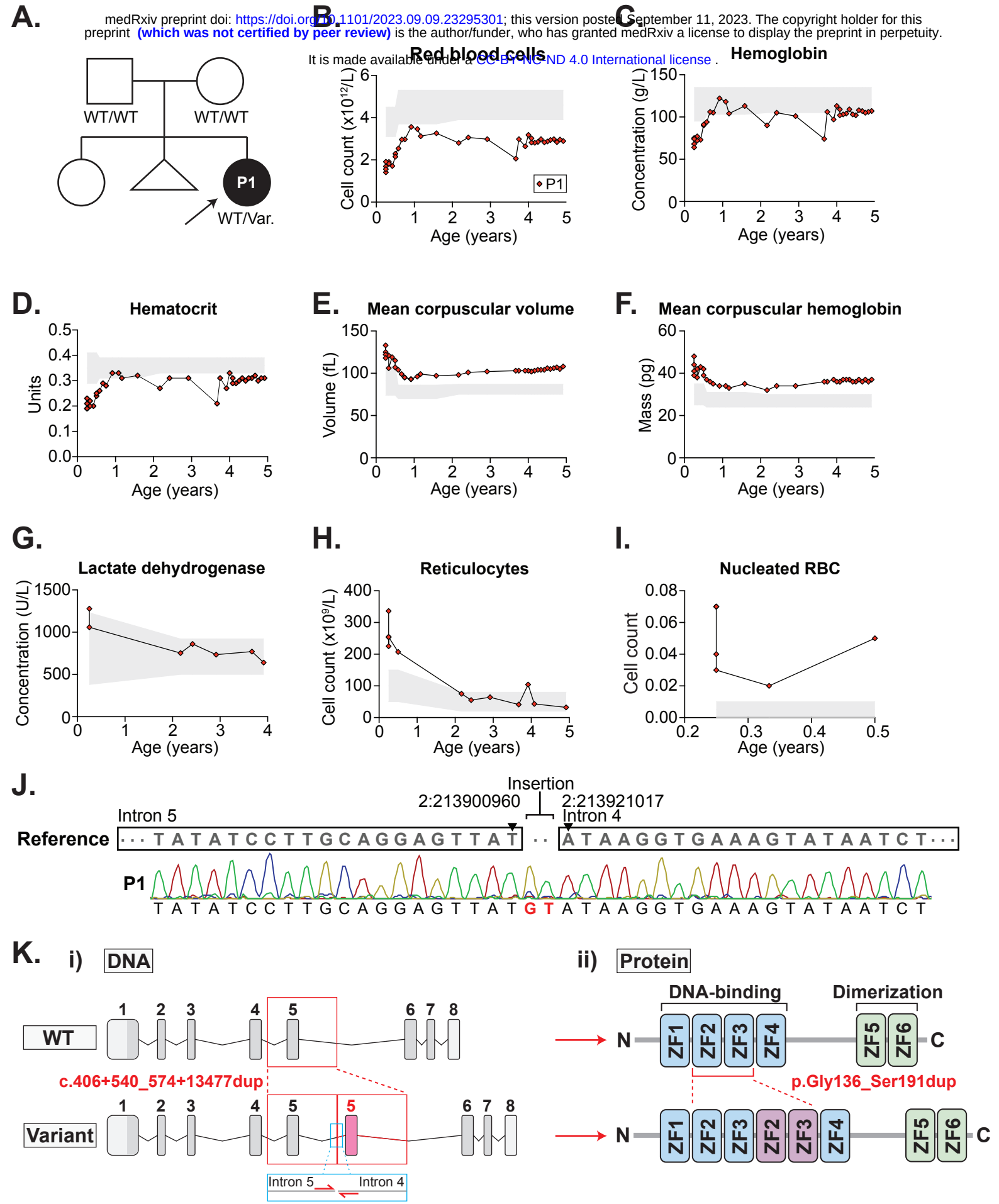

Figure 2

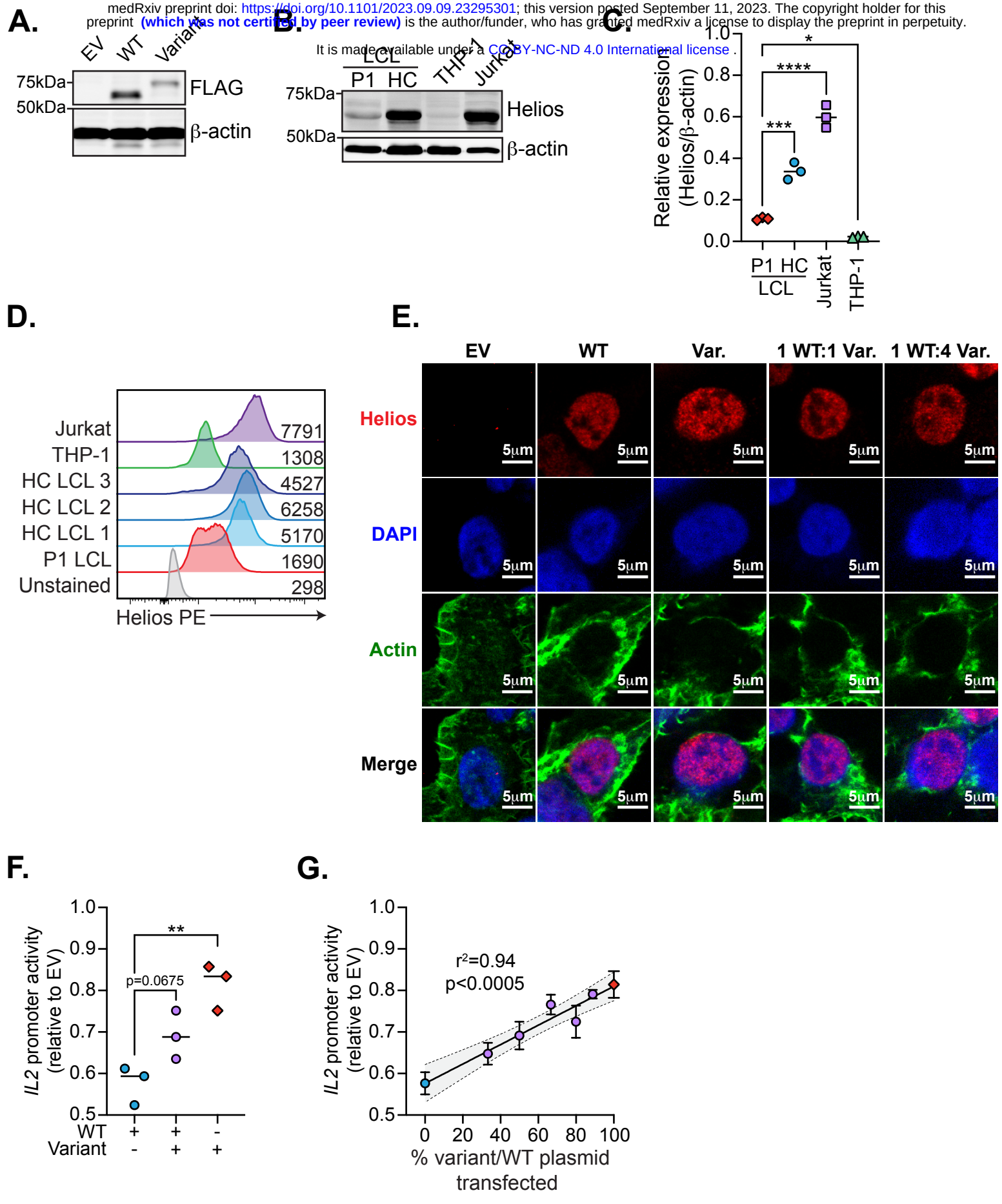

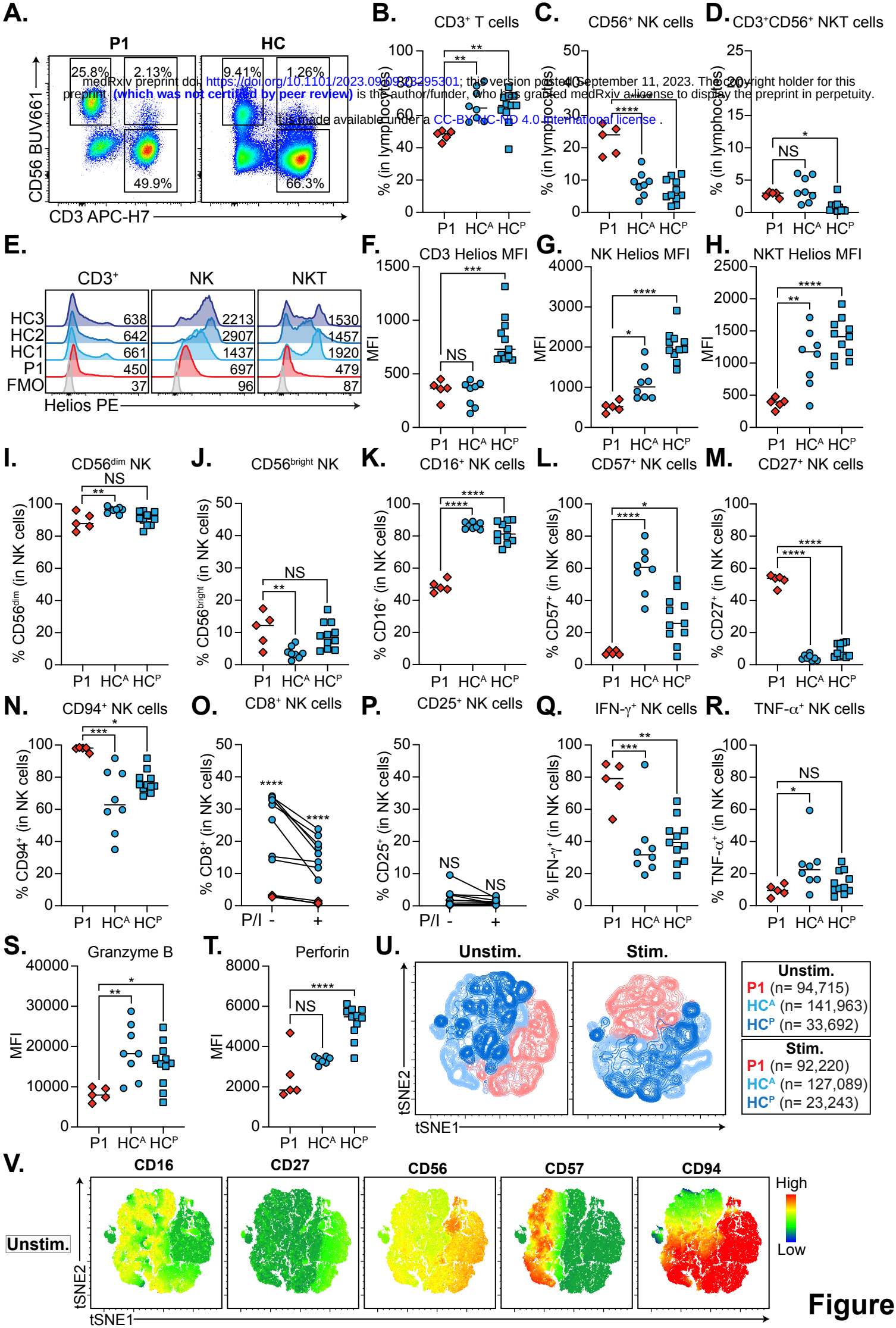

Figure 3

Figure 4

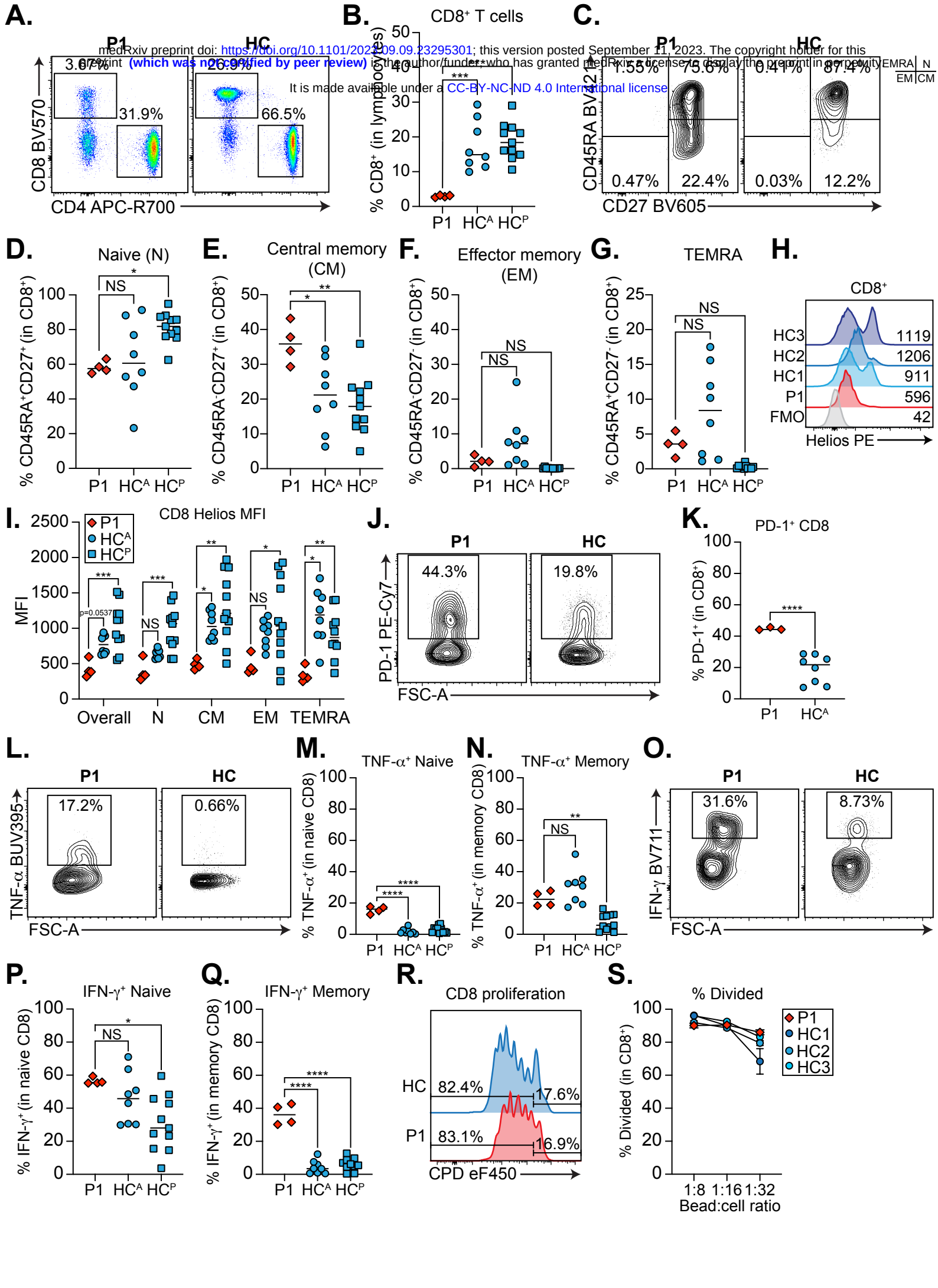

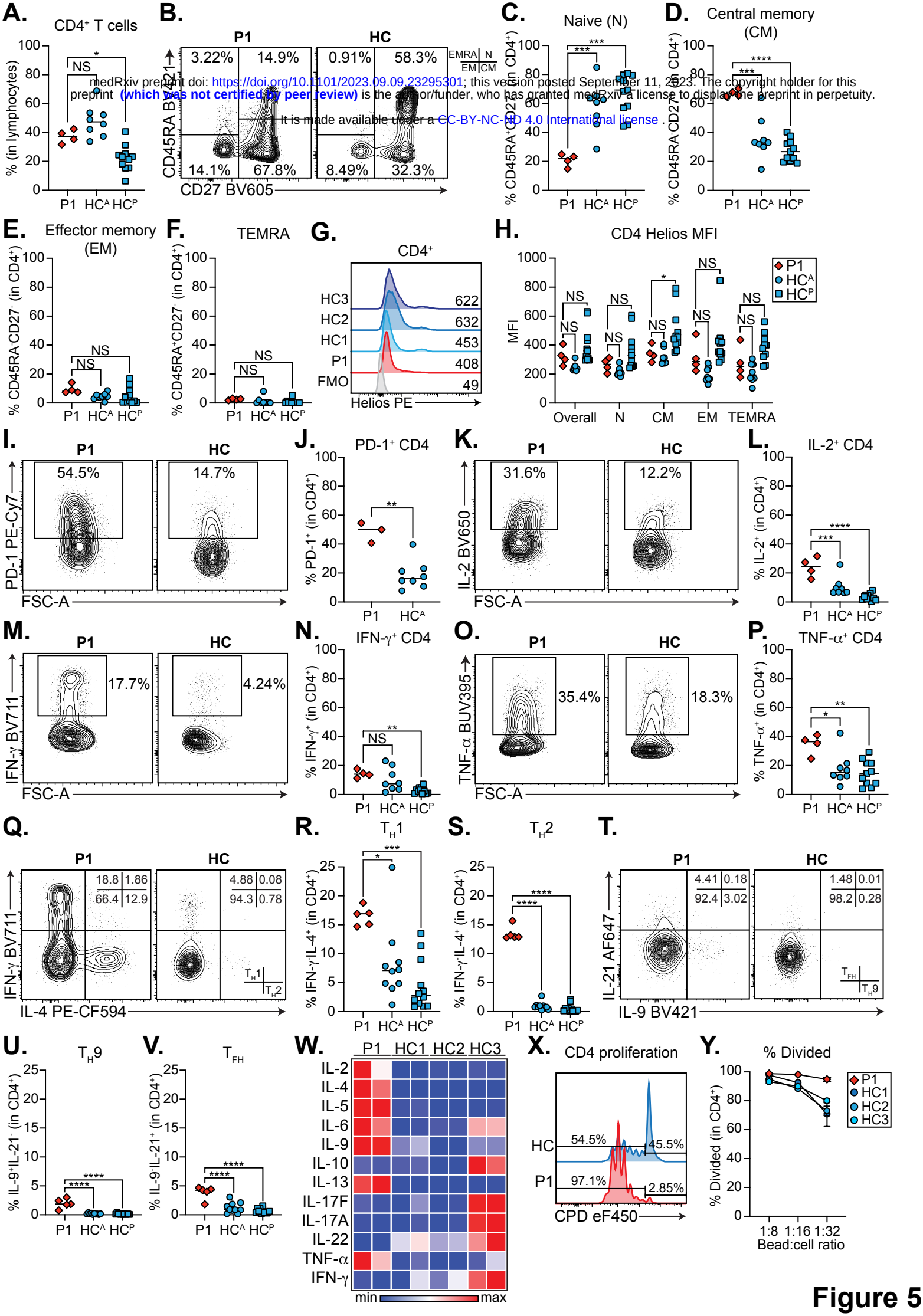

Figure 5

Figure 6

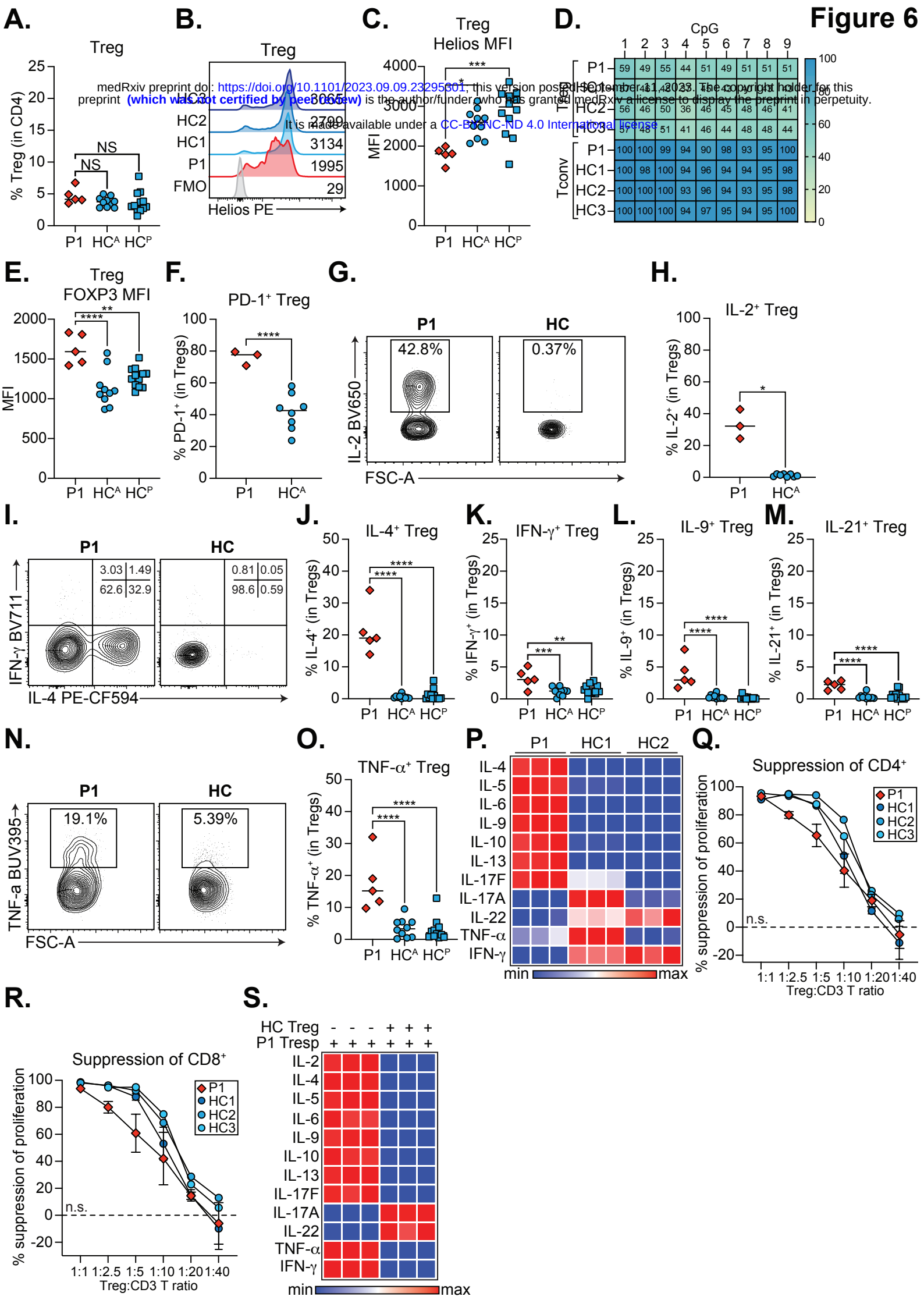

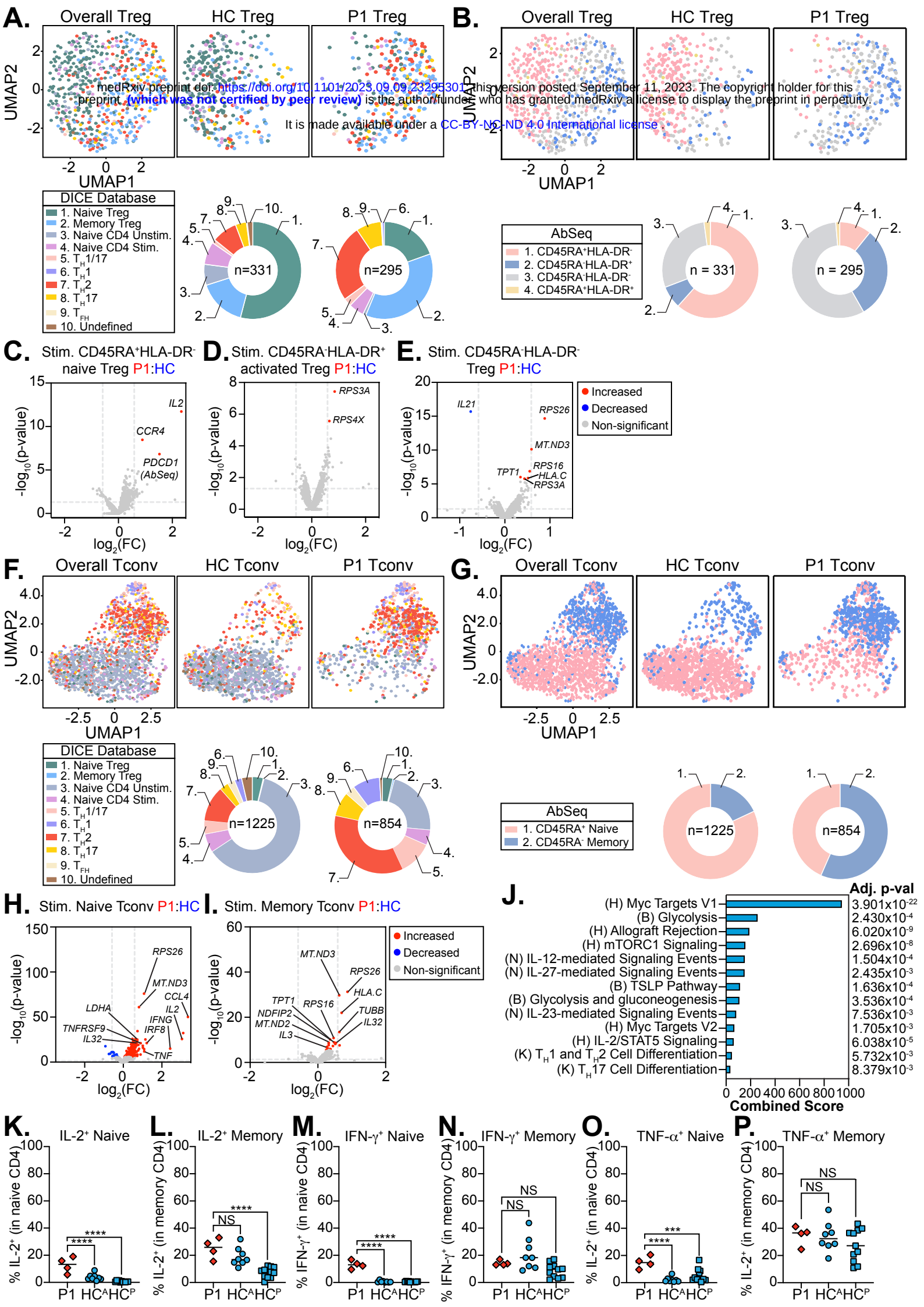

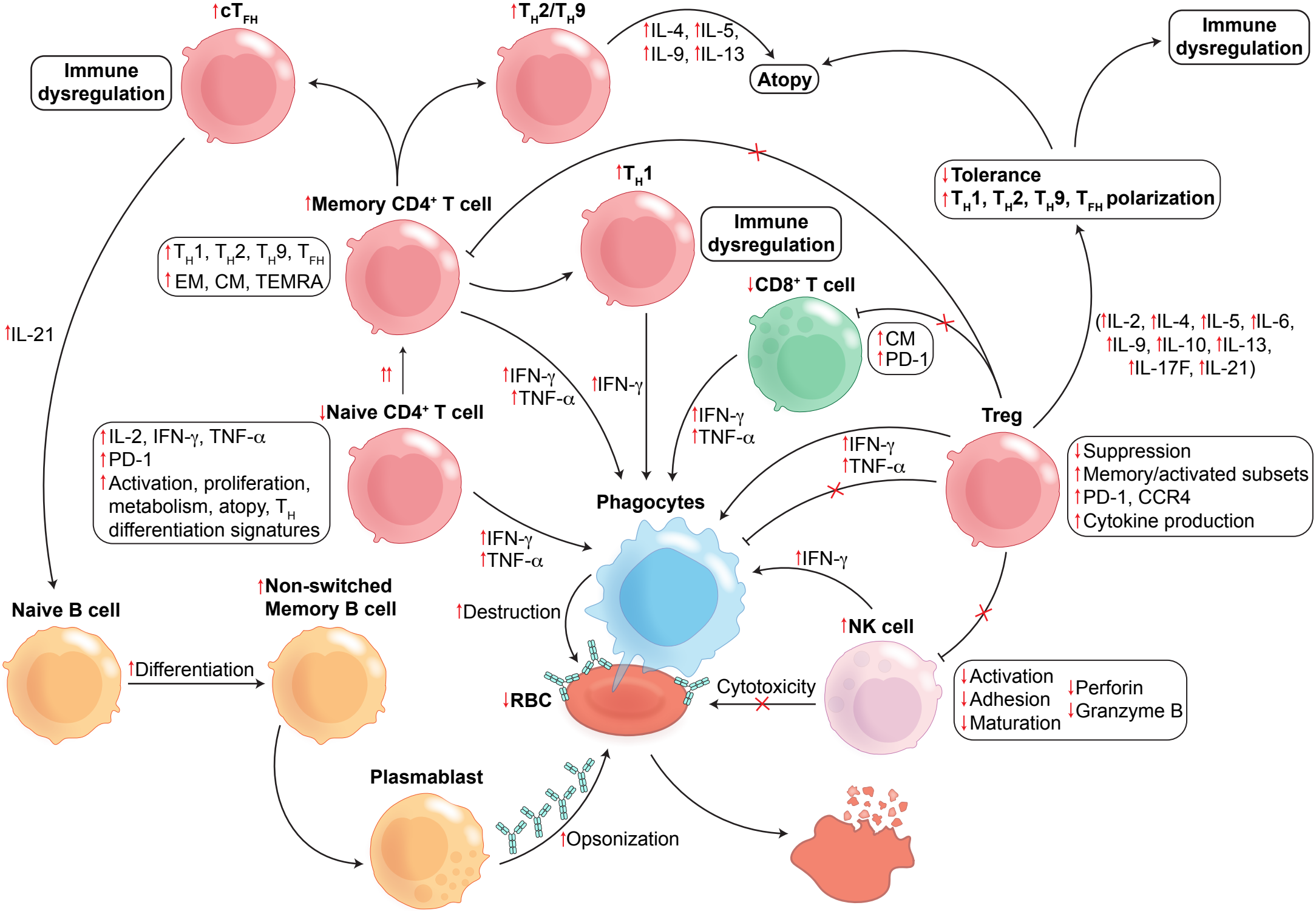
↑cT$_{FH}$
↑T$_H$2/T$_H$9
↑IL-4, ↑IL-5,
↑IL-9, ↑IL-13
Atopy
Immune dysregulation
Immune dysregulation
↓Tolerance
↑T$_H$1, T$_H$2, T$_H$9, T$_{FH}$ polarization
↑T$_H$1
↑Memory CD4$^+$ T cell
Immune dysregulation
↑T$_H$1, T$_H$2, T$_H$9, T$_{FH}$
↑EM, CM, TEMRA
↓CD8$^+$ T cell
↑CM
↑PD-1
(↑IL-2, ↑IL-4, ↑IL-5, ↑IL-6,
↑IL-9, ↑IL-10, ↑IL-13,
↑IL-17F, ↑IL-21)
↑IL-21
↑↑
↑IFN-γ
↑TNF-α
↑IFN-γ
↑IFN-γ
↑TNF-α
↓Naive CD4$^+$ T cell
Treg
↑IL-2, IFN-γ, TNF-α
↑PD-1
↑Activation, proliferation,
metabolism, atopy, T$_H$
differentiation signatures
↑IFN-γ
↑TNF-α
↓Suppression
↑Memory/activated subsets
↑PD-1, CCR4
↑Cytokine production
Phagocytes
↑IFN-γ
↑TNF-α
↑IFN-γ
↑Non-switched
Memory B cell
Naive B cell
↑Destruction
↑NK cell
↑Differentiation
↓RBC
Cytotoxicity
↓Activation
↓Adhesion
↓Maturation
↓Perforin
↓Granzyme B
Plasmablast
↑Opsonization

Table 1

	Patient (0.5-5 yo)	Reference (0.5-5 yo)
Lymphocytes (x10^9/L)	***1.31**	2.00 – 8.00
$CD3^+$ T cells	1.14	0.90 – 4.50
$CD4^+$ T cells	0.74	0.50 – 2.40
$CD8^+$ T cells	***0.19**	0.30 – 1.60
$CD19^+$ B cells	0.52	0.20 – 2.10
TREC (copy number / 3μL)	***3.08**	>75
Red blood cells (x10^{12}/L)	***2.83**	3.90 – 5.30
Reticulocytes (x10^9/L)	32	20-80
Nucleated red blood cells (x10^9/L)	***0.05**	<0.01
Platelets (x10^9/L)	383	200-490
Mean platelet volume (fL)	9.9	8.60 – 11.6
Neutrophils (x10^9/L)	3.07	1.50 – 8.50
Monocytes (x10^9/L)	0.54	0.00 – 0.90
Hemoglobin (g/L)	***103**	105 – 135
Hematocrit	***0.30**	0.33 – 0.39
Mean corpuscular volume	***104**	75 – 87
Mean corpuscular hemoglobin	***36**	24 – 30
Prothrombin time (s)	9.9	9.6 – 11.9
International normalized ratio	0.9	0.9 – 1.1
Lactate dehydrogenase (U/L)	640	500 – 920
Antibody Response		
IgG (g/L)	6.7‡	4.0 – 8.3
IgA (g/L)	0.63	0.18 – 1.00
IgM (g/L)	0.83	0.19 – 1.46
IgE (μg/L)	***242**	<18
Tetanus antitoxin (IU/mL)	0.83	0.10 – 1.00
Diptheria antitoxin (IU/mL)	0.70	0.50 – 1.10
DAT (polyspecific)	***Positive +3**	Negative
Anti-IgG	***Positive +3**	Negative
Anti-IgA	Negative	Negative
Anti-IgM	Negative	Negative
Anti-C3c	Negative	Negative
Anti-C3d	Negative	Negative
Hemoglobinopathy Workup		
HGB F	***0.044**	0.000 – 0.011
HGB A	***0.831**	0.848 – 0.920
HGB A2	0.029	0.022 – 0.034
BART's or HGB H Spike	Not detected	Not detected